The Astrophysical Journal Letters, 902:L9 (7pp), 2020 October 10 https://doi.org/10.3847/2041-8213/abb885

An Earth-like Stellar Wind Environment for Proxima Centauri c

Julián D. Alvarado-Gómez[1,7], Jeremy J. Drake[2,8], Cecilia Garraffo[2,3], Ofer Cohen[4], Katja Poppenhaeger[1,5], Rakesh K. Yadav[6], and Sofia P. Moschou[2]
[1] Leibniz Institute for Astrophysics Potsdam, An der Sternwarte 16, D-14482 Potsdam, Germany; julian.alvarado-gomez@aip.de
[2] Center for Astrophysics | Harvard & Smithsonian, 60 Garden Street, Cambridge, MA 02138, USA; jdrake@cfa.harvard.edu
[3] Institute for Applied Computational Science, Harvard University, Cambridge, MA 02138, USA
[4] University of Massachusetts at Lowell, Department of Physics & Applied Physics, 600 Suffolk Street, Lowell, MA 01854, USA
[5] University of Potsdam, Institute for Physics and Astronomy, Karl-Liebknecht-Str. 24/25, D-14476 Potsdam, Germany
[6] Department of Earth and Planetary Sciences, Harvard University, Cambridge, MA 02138, USA
Received 2020 August 4; revised 2020 September 11; accepted 2020 September 15; published 2020 October 7

Abstract

A new planet has been recently discovered around Proxima Centauri. With an orbital separation of ∼1.44 au and a minimum mass of about 7 $M_{\oplus}$, Proxima c is a prime direct imaging target for atmospheric characterization. The latter can only be performed with a good understanding of the space environment of the planet, as multiple processes can have profound effects on the atmospheric structure and evolution. Here, we take one step in this direction by generating physically realistic numerical simulations of Proxima's stellar wind, coupled to a magnetosphere and ionosphere model around Proxima c. We evaluate their expected variation due to the magnetic cycle of the host star, as well as for plausible inclination angles for the exoplanet orbit. Our results indicate stellar wind dynamic pressures comparable to present-day Earth, with a slight increase (by a factor of 2) during high-activity periods of the star. A relatively weak interplanetary magnetic field at the distance of Proxima c leads to negligible stellar wind Joule heating of the upper atmosphere (about 10% of the solar wind contribution on Earth) for an Earth-like planetary magnetic field (0.3 G). Finally, we provide an assessment of the likely extreme conditions experienced by the exoplanet candidate Proxima d, tentatively located at 0.029 au with a minimum mass of 0.29 $M_{\oplus}$.

Unified Astronomy Thesaurus concepts: Stellar winds (1636); Stellar magnetic fields (1610); Planetary magnetosphere (997); Stellar mass loss (1613); Interplanetary magnetic fields (824); Stellar activity (1580); Super Earths (1655); Exoplanets (498)

1. Introduction

The space weather in M dwarf planetary systems presents a particularly challenging case for exoplanet atmospheres. The diminutive bolometric luminosity ($L_{\rm bol}$) of M dwarfs means their temperature-based habitable zones, within which liquid water can be sustained, lie close to the central star—as much as 10 or more times closer than in the case of our own solar system (e.g., Kopparapu et al. 2013, 2014; Shields et al. 2016).

Specifically, the habitable zone semimajor axis (a) follows $a^2 \propto L_{\rm bol}$ (Kopparapu et al. 2013). On the other hand, stellar wind mass-loss rates are thought to scale with X-ray luminosity with a power greater than one (i.e., $\dot{M}_{\star} \propto L_{\rm X}^{1.34}$; Wood et al. 2005). In this way, the wind through a unit surface area at the main-sequence habitable zone distance scales like $\dot{M}_{\star}/a^2 \propto L_{\rm X}^{1.34}/L_{\rm bol} \propto L_{\rm X}^{1.34}/M_{\star}^{3.5}$. Therefore, the stellar wind intensity within the habitable zone increases with decreasing stellar mass. Moreover, M dwarfs remain magnetically very active (i.e., high $L_{\rm X}/L_{\rm bol}$ values) over much longer timescales than higher-mass stars (e.g., Wright et al. 2011; Davenport et al. 2019), so that the integrated exposure to the most intense stellar winds is commensurately greater.

A number of studies employing detailed and realistic magnetohydrodynamic (MHD) simulations of stellar winds have examined the effects of space weather on exoplanets, including those in M dwarf systems (e.g., Cohen et al. 2014; Vidotto et al. 2014; Alvarado-Gómez et al. 2019b). For habitable zone planets around M dwarfs, models predict stellar wind dynamic pressures up to four orders of magnitude greater than experienced by the present-day Earth, together with orders of magnitude pressure variations on sub-orbital timescales of one to a few days (Vidotto et al. 2014, Garraffo et al. 2016, 2017), intense Joule heating (Cohen et al. 2014, 2018), severe atmospheric loss (Dong et al. 2017; Garcia-Sage et al. 2017), and transitions into and out of sub-Alfvénic wind conditions on orbital timescales (Cohen et al. 2014; Garraffo et al. 2017).

Here, we study the steady stellar wind environment of the newfound planetary companion around our nearest star (Proxima c; Damasso et al. 2020). The discovery of a planetary system around Proxima (Anglada-Escudé et al. 2016) represented a watershed moment in exoplanetary research—a stark confirmation that planetary systems are very common in the universe with the tantalizing prospect of potentially being reachable by an interstellar probe (e.g., Heller et al. 2017; Parkin 2018). We construct three-dimensional MHD models of the magnetized stellar wind of Proxima using a state-of-the-art computational framework and a surface magnetic field map derived from sophisticated dynamo simulations tuned to the case of Proxima (Yadav et al. 2016).

We use the models to investigate the conditions experienced by Proxima c, which is estimated to have a mass of about 7 times that of Earth, orbiting at a distance comparable to Mars in

[7] Karl Schwarzschild Fellow.

the solar system (Damasso et al. 2020). We evaluate how the stellar wind properties change with the magnetic activity level of the host star, and compare our results to those of previous studies on other exoplanet systems. Finally, we touch upon the case of Proxima d, a tentative additional planetary candidate of the Proxima system that would be the closest known planet to the star, lying within the orbit of Proxima b (Suárez Mascareño et al. 2020).

2. The Proxima Centauri System

Proxima Centauri, also just known as Proxima, is an M5.5 dwarf with an effective temperature of 3042 K, a mass of 0.122 $M_\odot$, a radius of 0.154 $R_\odot$, a rotation period of 83 days, and an estimated age of 4.85 Gyr (Ségransan et al. 2003; Kiraga & Stepien 2007; Anglada-Escudé et al. 2016).

Proxima hosts our nearest exoplanetary system and presents a unique opportunity for exoplanet characterization. The first planet discovered in the system, Proxima b, is estimated to be of at least 1.17 Earth masses (Suárez Mascareño et al. 2020) and has an orbital period of 11.2 days, with a semimajor axis of only 0.049 au (Anglada-Escudé et al. 2016). This orbit is approximately 20 times closer to Proxima than the Earth is to the Sun. Proxima b does not transit Proxima Centauri from the vantage point of the solar system (Jenkins et al. 2019) and its orbital inclination and, consequently, its mass are presently unknown.

Proxima b is in Proxima's classically defined "habitable zone," having an equilibrium temperature of 234 K (Anglada-Escudé et al. 2016), which is slightly cooler than that of Earth (255 K). Several studies have examined its likely irradiation history and possible climate and evolution in relation to potential habitability (e.g., Ribas et al. 2016; Turbet et al. 2016).

Analysis of radial velocity variations by Damasso et al. (2020) suggested the presence of a secondary ∼6–7 $M_\oplus$ planet in a ∼5 yr orbit around Proxima. Follow-up studies have placed limits on the properties of Proxima c, measuring anomalies in Proxima's astrometric proper motion (Benedict & McArthur 2020a; Kervella et al. 2020), as well as direct imaging from ground-based observations (Gratton et al. 2020). Combining all the available constraints, (Benedict & McArthur 2020b) obtained the most up-to-date set of orbital parameters, placing it in a circular orbit ($e \simeq 0$) at approximately 1.44 au (∼5.3 yr orbital period).

A recent study reports a small radial velocity perturbation of Proxima that, assuming a planetary origin, would indicate an additional low-mass object ($M \sin i \simeq 0.29\ M_\oplus$) at a distance of ∼0.029 au (Suárez Mascareño et al. 2020). If confirmed, it would become the innermost known planet of the system, orbiting closer than Proxima b and just short of the optimistic habitable zone (∼0.03–0.09 au; Kane & Gelino 2012).

Harsh circumstellar conditions are expected in the system. Proxima itself is a flare star and displays optical, UV, and X-ray variability that is consistent with a stellar activity cycle with a period of about 7 years (Wargelin et al. 2017). The amplitude of the cycle in the stellar X-ray luminosity is of the order of ±50% in an energy band of 1.2–2.4 keV, and somewhat lower in softer X-rays at energies 0.2–1.2 keV at approximately ±20%. This means that apart from flares, which occur often on Proxima (e.g., Fuhrmeister et al. 2011; Vida et al. 2019), the quiescent X-ray environment of the planets also changes over time.

Unlike the coronal properties, only limits are available on the steady and transient outflows from Proxima. Observations of the Lyα astrospheric absorption indicate a stellar wind mass-loss rate[8] $\dot{M}_\star < 0.2\ \dot{M}_\odot$ (Wood et al. 2001), while wind–interstellar medium (ISM) charge exchange X-ray signatures place it at $\dot{M}_\star < 14\ \dot{M}_\odot$ (Wargelin & Drake 2002). Likewise, despite its frequent flaring, there are no direct detections of coronal mass ejections in Proxima so far (see Moschou et al. 2019 and references therein).

3. Numerical Methodology

Our characterization of the stellar wind conditions in the Proxima Cen system employs the state-of-the-art Space Weather Modeling Framework (SWMF; Gombosi et al. 2018). Originally developed for solar system studies, the SWMF contains a collection of physics-based models that can be executed individually or can be coupled to cover a wide range of regions within the space environment of the Sun (e.g., from the convection zone to the outer heliosphere; see Tóth et al. 2012). The simulations presented here consider four modules of the SWMF, covering the stellar corona (SC; ∼1.0–110 $R_\star$), the inner heliosphere[9] (IH; 105–2250 $R_\star$), the global magnetosphere[10] (GM; dayside: 100 R_p, nightside: 225 R_p, north–south: 256 R_p), and a domain for ionospheric electrodynamics[11] (IE).

The multidomain solution is constructed from inside out, initially calculated within the SC module using the Alfvén Wave Solar Model (AWSoM; van der Holst et al. 2014), whose standard boundary conditions are modified to the M dwarf regime (and specifically for Proxima) as described in Alvarado-Gómez et al. (2020). In particular, two surface magnetic field configurations—associated with minimum and maximum activity—are considered to drive individual AWSoM solutions. These have been extracted[12] from a self-consistent fully convective dynamo simulation—adjusted to the stellar mass, radius, and rotation period of Proxima (see Yadav et al. 2016)—whose oscillatory regime yields a timescale comparable with the observed activity cycle in the star (Section 2). As shown in the top panels of Figure 1, we scale the average surface field strengths for activity minimum (450 G) and maximum (750 G) to match the limits from Zeeman broadening observations of Proxima ($\langle B \rangle_S = 600 \pm 150$ G; Reiners & Basri 2008).

Once an AWSoM steady state is achieved, it gets propagated via three different couplings with the other domains. The first one connects the outer boundary of SC with the inner boundary of IH (with a 5 $R_\star$ domain overlap), while the second one is performed within the IH domain (along the specified orbit of Proxima c) establishing the upstream stellar wind conditions as one of the outer (side) boundaries of the GM. As the magnetosphere relaxes, the third coupling takes place, where field-aligned currents are computed in the GM, and then are mapped to the IE domain assuming a planetary dipole field of −0.3 G (aligned with z-axis) in the case of Proxima c. We stress here that there are no observational constraints on the magnetization of this exoplanet. The planetary field selection was made to ease the comparison with the case of the Earth and other systems studied with a similar methodology (e.g.,

[8] Assuming $\dot{M}_\odot \simeq 2 \times 10^{-14}\ M_\odot\ \mathrm{yr}^{-1} = 1.265 \times 10^{12}\ \mathrm{g\ s}^{-1}$.

[9] Denoted as inner astrosphere in the stellar case.

[10] The domain size is defined in units of planetary radii instead of stellar radii in this case.

[11] A two-dimensional sphere set at an altitude of 120 km in the case of the Earth.

[12] Rotations 508 (minimum) and 520 (maximum) from the Yadav et al. (2016) study are used for this purpose.

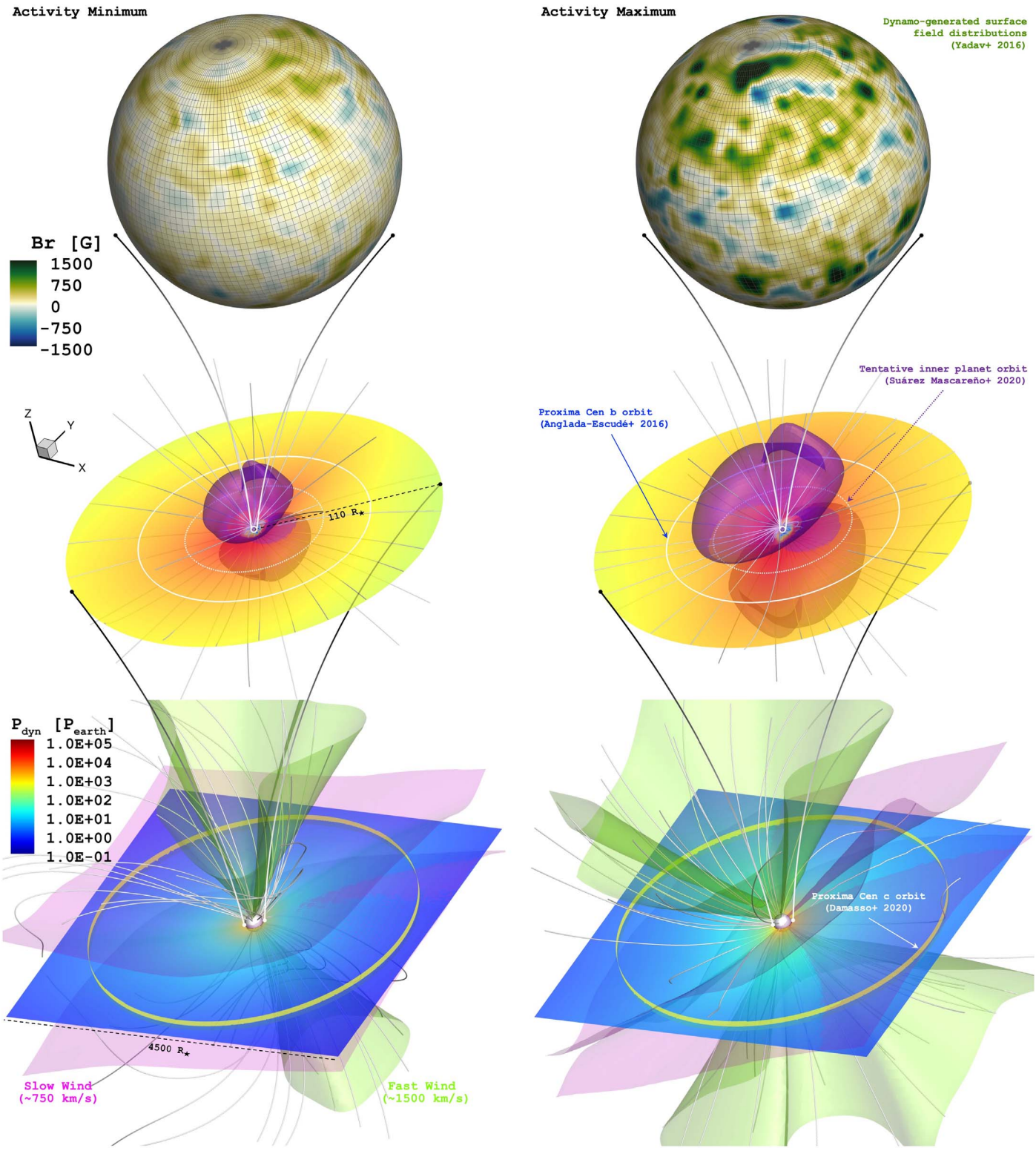

Figure 1. Simulated stellar wind environment for the Proxima Cen system. Multidomain models for activity minimum (left) and maximum (right) are shown. The top panels contain the dynamo-generated surface field distributions (in G) used to drive the AWSoM solution within the innermost module (SC; middle panels). This domain contains the orbits of Proxima b (white solid) and the tentative innermost planet Proxima d (white dashed). The purple isosurface corresponds to the Alfvén surface of the stellar wind ($M_A = 1$; see the text for details). The steady-state solution is propagated from the coupling region (105–110 $R_\star$) to the entire IH domain (4500 $R_\star$ in each Cartesian direction; bottom panels). This domain contains the orbit of Proxima c (yellow). Magenta and green isosurfaces delimitate the slow ($U_r \lesssim 750$ km s^{-1}) and fast ($U_r \gtrsim 1500$ km s^{-1}) wind sectors, respectively. Color-coded is the wind dynamic pressure ($P_{dyn} = \rho\, U^2$) normalized to the nominal Sun–Earth value (~ 1.5 nPa), visualized on the equatorial plane of both domains. Selected magnetic field lines are shown in white.

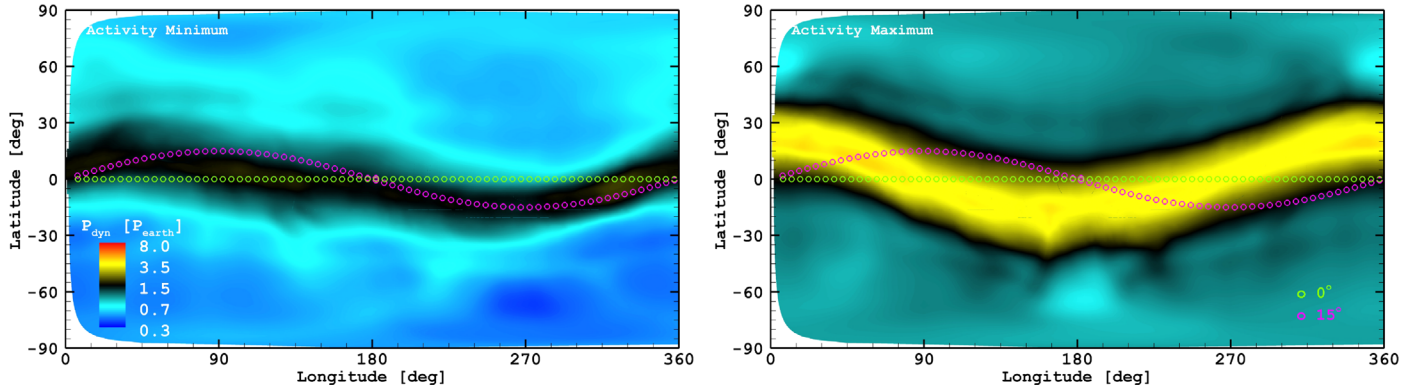

Figure 2. Two-dimensional Mercator projection of the normalized stellar wind dynamic pressure ($P_{\rm dyn}$), extracted from a sphere at the distance of Proxima c ($\sim$1.44 au $\simeq$2010.39 $R_\star$). Green and magenta dotted lines indicate the path for 0° and 15° orbital inclinations, respectively. Conditions for activity minimum (left) and maximum (right) are shown.

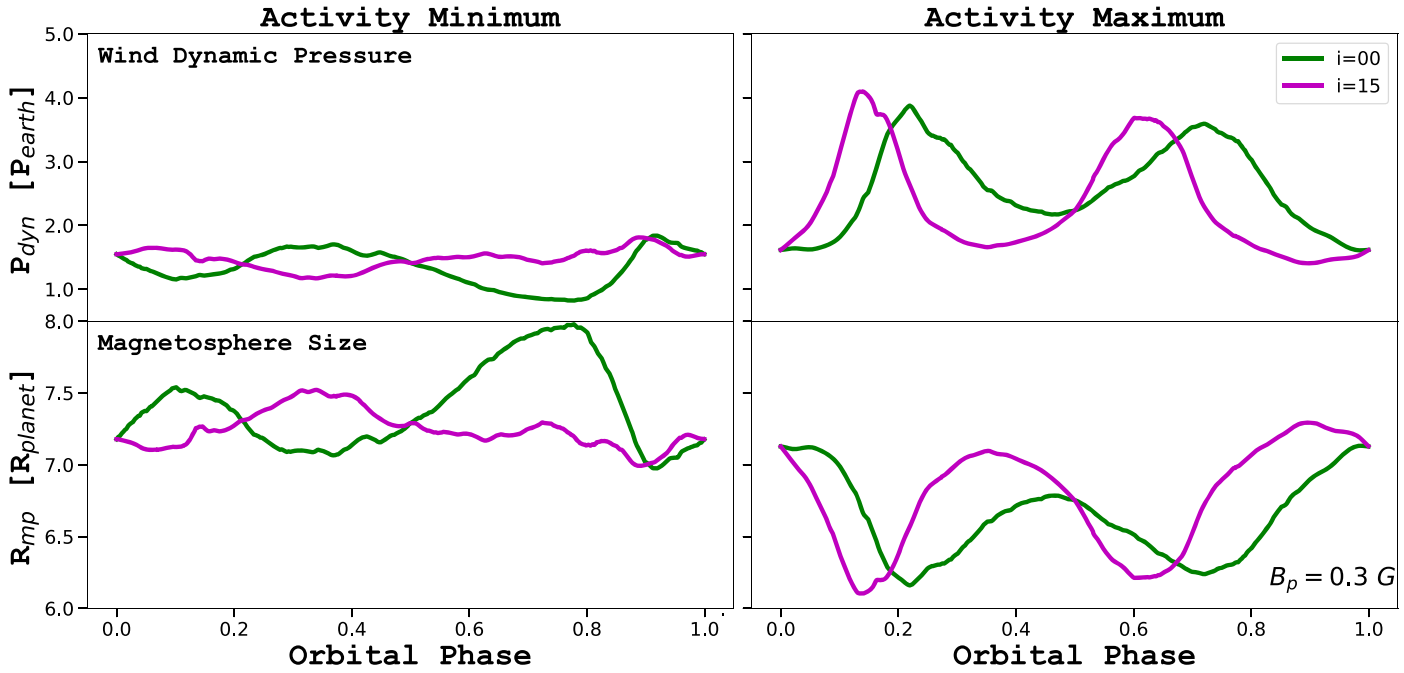

Figure 3. Variation of the normalized wind dynamic pressure ($P_{\rm dyn}$; top) and the magnetosphere size ($R_{\rm mp}$; bottom) along possible orbits of Proxima c. Green and magenta lines show the behavior for orbital inclinations of 0° and 15°, respectively (see Figure 2). Conditions for both stellar activity states are included (minimum: left, maximum: right). An Earth-like planetary dipole magnetic field ($B_{\rm p}$ = 0.3 G) is assumed in all cases.

Alvarado-Gómez et al. 2019b; Cohen et al. 2020). The IE module uses the field-aligned currents to calculate the flux of the precipitating electrons, and the energy dissipating in the ionosphere (Joule heating, hereafter JH) assuming a specific conductance pattern that can be either a constant Pedersen conductivity, or a more complicated conductivity pattern that can be obtained from other models or data. In the Earth case, the integrated conductivity ranges between 1 S and 10 S, where a lower value leads to an increased JH (Cohen et al. 2014). For simplicity, we use a constant conductivity of 1 S to estimate an upper limit to the JH under the assumed stellar wind parameters. The IE provides improved boundary conditions for GM in the form of electric and velocity fields at the inner boundary. We refer the reader to Cohen et al. (2020) for more details about the GM–IE coupling, and the JH calculation.

A combination of spherical (SC) and Cartesian (IH/GM) grids is employed, which is further optimized using multiple realizations of adaptive mesh refinement/coarsening, informed by magnetic field and particle density gradients. This was necessary to keep the number of cell blocks tractable, given the very large IH box size (side length: 4500 $R_\star$) required to contain the complete orbit of Proxima c ($a \simeq 2010.39\,R_\star$, $e = 0.0$; see Benedict & McArthur 2020b; Damasso et al. 2020). In this way, the combined domain contains more than 24 million spatial blocks, with the smallest cell elements in the final mesh reaching 0.025 $R_\star$ (SC), 4.394 $R_\star$ (IH), and 0.3 $R_{\rm p}$ (GM).

4. Results and Discussion

Results from our numerical simulations of the Proxima system are presented in Figures 1–4, where side-by-side visualizations for activity minimum and maximum are shown. As described below, good agreement is obtained with current observational constraints on Proxima's stellar wind, as well as with previous modeling work by Garraffo et al. (2016) on the space weather conditions around Proxima b (Figure 1, middle panels).

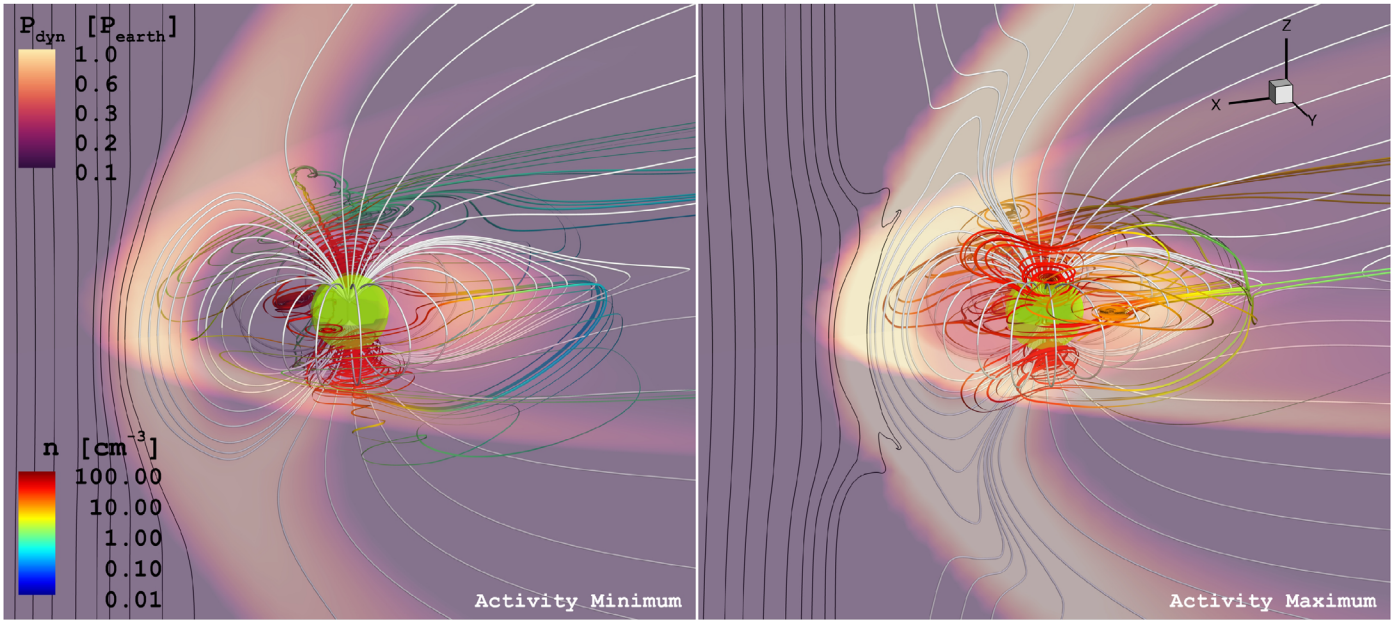

Figure 4. Results from the GM+IE model driven by stellar wind parameters representative of both activity states (minimum: left, maximum: right; see Table 1), extracted from the analyzed orbits of Proxima c within the IH module (Figures 1 and 2). The star is located in the positive x direction and the central sphere (green) corresponds to the inner boundary of the domain ($R = 2\,R_p$). Equatorial and meridional projections of the normalized wind dynamic pressure are included (P_{dyn}, burgundy). Randomly seeded velocity streamlines, color-coded by plasma number density (n, rainbow), are used as proxy for particle trajectories inside the magnetosphere. Selected stellar wind (black) and planetary (white) magnetic field lines are shown.

4.1. Stellar Wind Models

Despite the differences in surface field strength and topology (Figure 1, top panels), the resulting steady-state wind solutions are similar between both activity states. This is a consequence of comparable large-scale magnetic field components among both configurations, with the small-scale structure mostly controlling the coronal thermodynamic conditions (see Garraffo et al. 2015; Réville et al. 2015). The associated Alfvén surface (AS)[13] displays a characteristic two-lobe configuration (Figure 1, middle panels), with average sizes of 28.1 $R_\star$ and 46.5 $R_\star$ for activity minimum and maximum, respectively. The wind distribution is mainly bipolar (see Figure 1, bottom panels), with a relatively fast component reaching up to $\sim$1500 km s^{-1} in the (magnetic) poleward directions, and a slow wind sector ($\lesssim$750 km s^{-1}) surrounding the astrospheric current sheet. The latter is roughly aligned with the equatorial plane during minimum, gaining a small inclination angle ($\sim 20°$) for activity maximum.

Computing the stellar wind mass-loss rate for each magnetic configuration yields $\sim$0.3 $\dot{M}_\odot$ (minimum) and $\sim$0.9 $\dot{M}_\odot$ (maximum). These values appear close to current upper limits from observations (see Section 2). Note also that the factor of 3 difference in $\dot{M}_\star$ between activity states is comparable to the observed variation in $\dot{M}_\odot$ over the solar cycle (by a factor of $\sim$2; Finley et al. 2018).

4.2. Stellar Wind Environment of Proxima c

Having established that our simulations provide a robust description of Proxima's stellar wind, we now proceed to assess the expected conditions for planet c. For each activity state, the bottom panels of Figure 1 display the resulting stellar wind dynamic pressure, $P_{dyn} = \rho\, U^2$ (normalized to the average value experienced by the Earth,[14] $P_{earth} \simeq 1.5$ nPa), up to the orbital distance of Proxima c.

To examine their expected orbital variations, Figure 2 shows two-dimensional Mercator projections of P_{dyn} constructed from a sphere with the radius matching the semimajor axis of Proxima c ($\sim$1.44 au). We include the orbital paths for two possible inclinations[15] of the planet (0° and 15°). During minimum, the largest value in P_{dyn} along the explored orbits is close to 2 times the Sun–Earth average. The conditions worsen slightly for activity maximum, with a stellar wind dynamic pressure reaching up to 4 P_{earth}.

For the considered inclinations, the orbital variability of P_{dyn} is rather small, being around 50% for activity minimum and close to a factor of 2 during maximum. This is better illustrated in the top panels of Figure 3, showing the behavior of P_{dyn} as a function of orbital phase in all cases. With a more inclined orbit, Proxima c would be exposed to stellar wind sectors of substantially lower dynamic pressure, at the cost of enhanced variability during each current sheet crossing (e.g., Alvarado-Gómez et al. 2016; Garraffo et al. 2016).

Interestingly, our P_{dyn} results for Proxima c are comparable with expectations for Barnard Star b (see Alvarado-Gómez et al. 2019b), which resides much closer to its host star ($a \simeq 0.4$ au, $e \simeq 0.32$; Ribas et al. 2018). At a considerable older age ($\sim$10 Gyr), the weaker magnetism of Barnard Star creates a slower and more rarefied stellar wind compared to Proxima. This compensates the shorter orbital distance, leading to similar P_{dyn} conditions for both super-Earth planets.

The super-Alfvénic stellar wind conditions along the orbit, combined with the assumption of a dipole planetary magnetic

[13] Defined by the locations in which the stellar wind speed matches the local Alfvén speed (i.e., an Alfvénic Mach number $M_A = U\sqrt{4\pi\rho}/B = 1$, where U, ρ, and B correspond to the wind speed, density, and magnetic field values, respectively).

[14] https://www.swpc.noaa.gov/products/real-time-solar-wind

[15] Measured with respect to the equatorial plane and not with respect to the line of sight (which is the value reported in Kervella et al. 2020 and Benedict & McArthur 2020b).

Table 1
Representative Stellar Wind Parameters around Proxima c and Resulting Properties from the GM+IE Modules

Case	Incident Stellar Wind				Global Magnetosphere (GM+IE)		
	n [cm^{-3}]	T [$\times 10^4$ K]	$\boldsymbol{U}$ [km s^{-1}]	$\boldsymbol{B}$ [nT]	R_{mp}^{min} [R_p]	P_{mp}^{max} [P_{earth}]	JH [JH$_{earth}$]
Minimum	1.0	5.0	(−1100, 0, 0)	(0, 0, −0.5)	8.2	1.3	0.07
Maximum	10.0	10.0	(−600, 0, 0)	(0, 0, −2.0)	6.2	2.4	0.16

field (B_p), allow a broad estimate on the associated day-size magnetosphere size (R_{mp}). This is done by considering the magnetic and stellar wind dynamic pressure balance (e.g., Schield 1969; Gombosi 2004) leading to the relation

$$\frac{R_{mp}}{R_p} = \left(\frac{B_p^2}{8\pi P_{dyn}}\right)^{1/6}. \quad (1)$$

Assigning an Earth-like dipole magnetic field $B_p = 0.3$ G to Proxima c, this calculation yields a magnetosphere size ranging between ∼6–8 R_p among both activity states (see Figure 3, bottom panels). These values appear close to the standard size of the dayside Earth's magnetosphere (∼10R_{earth}), which can be compressed by up to ∼35% during strong solar space weather events (see Pulkkinen 2007; Lugaz et al. 2015). Figure 3 also shows the inverse relation between the dynamic pressure and the magnetosphere size, with crossings of the current sheet as coinciding peaks and dips in P_{dyn} and R_{mp}, respectively. As can be seen from Equation (1), $R_{mp} \propto B_p^{1/3}$, so that larger magnetosphere sizes are expected for stronger planetary magnetic field values.

To complement the analytic description, our multidomain simulation also includes a three-dimensional model of a possible magnetosphere and ionosphere around Proxima c (see Section 3). We evaluate the stellar wind properties along the considered orbits of Proxima c in order to obtain nominal conditions—namely, density, speed, magnetic field strength, and temperature—in each activity state (see Table 1). These representative stellar wind parameters are used to drive the GM and IE modules, whose results are presented in Figure 4. The visualizations include equatorial and meridional projections of P_{dyn}, clearly showing the development of a bow shock toward the star (positive x-axis). As expected, the harsher stellar wind conditions during maximum generate higher compression of the entire magnetosphere compared to activity minimum. In combination with the polarity and strength of the interplanetary magnetic field, this will influence the fraction of particles penetrating and precipitating to the ionosphere (illustrated in Figure 4 by density-colored velocity streamlines). A summary of the resulting values from the GM module is presented in Table 1. Note that the smallest magnetosphere standoff distance from GM is fairly consistent with the analytic formulation given by Equation (1) (see also Figure 3, bottom panels).

Following Cohen et al. (2020), we calculate the associated Joule heating in the upper atmosphere using the IE model. We find that the Joule heating is very low for both activity states—about ∼10% of the heating obtained at Earth during ambient solar wind conditions (JH $_{earth} \simeq 150$ GW; see Table 1). The reason for this is that while P_{dyn} is higher for Proxima c than for the Earth, the average solar wind conditions carry a stronger magnetic field (particularly in the B_z component), whose variations ultimately drive the field-aligned currents and the particle influx responsible for the JH. Previous studies of the TRAPPIST-1 planets (Cohen et al. 2018) and TOI-700 d (Cohen et al. 2020) indicate much higher values of JH that could potentially contribute to continuous heating of the upper atmosphere of these planets. However, such heating is likely negligible for Proxima c.

4.3. Extreme Conditions for Proxima d

To complete this study, we examine the expected space environment around the planet candidate Proxima d. As mentioned in Section 2, its ∼40.4 $R_\star$ orbit would place it closer than Proxima b ($a \simeq 67.8\ R_\star$), exposing it to even more extreme conditions than the habitable zone planet. This includes P_{dyn} values about 5 times larger than expectations for Proxima b[16] (Garraffo et al. 2016), corresponding to 3–4 orders of magnitude larger than what the present-day Earth experiences (see Figure 1, middle panels). While both exoplanets would face similar intra-orbital variations in P_{dyn} (by a factor of ∼10), they will occur approximately twice as fast in Proxima d compared to b (∼5.2 day versus ∼11.2 day orbital periods). Furthermore, the 46.5 $R_\star$ average size of the AS during maximum—larger than the orbital separation—implies that Proxima d would cross (or be completely in) sub-Alfvénic stellar wind sectors at times of high activity in the star. Leaving aside the increased rate of high-energy transients and their expected strong coronal response on Proxima (see Alvarado-Gómez et al. 2019a), the sub-Alfvénic conditions pose an even greater challenge for the retention of any atmosphere around the planet (e.g., analogous to the case of the TRAPPIST-1 system; Garraffo et al. 2017; Cohen et al. 2018).

5. Summary and Conclusions

As the closest planetary system to Earth, Proxima Centauri and its circumstellar properties are of great importance for exoplanet and habitability studies. To characterize the expected conditions of the recently discovered Proxima c, we have constructed the most comprehensive numerical simulation of the space environment in this system to date. This includes coupled models for the stellar corona and inner astrosphere—where the complete ∼1.44 au orbit of the planet is enclosed—driven by realistic surface magnetic field configurations representative of the minimum and maximum activity states of Proxima.

Our results indicate that Proxima c experiences Earth-like conditions—in terms of the dynamic pressure exerted by the stellar wind—along its ∼5.3 yr orbit, with minor variability (by a factor of ∼2) due to the activity cycle of the star. To investigate the relative effect of such conditions on the energy dissipation in the upper atmosphere (Joule heating), we also simulated a possible magnetosphere and ionosphere around the planet. We found that even with a relatively weak planetary dipole field (0.3 G), the associated Joule heating of the upper atmosphere is negligible for Proxima c (∼10% of the nominal value on the Earth), due to a diminished interplanetary magnetic field at the distance of the

[16] Comparing with the $\langle B \rangle_S = 600$ G case from Garraffo et al. (2016).

planet. Whether or not Proxima Cen c currently has an atmosphere would depend on several factors, including its formation channel and evolutionary path. Nevertheless, at face value the resulting conditions from our models do not appear to be unduly corrosive and should be favorable for the persistence of any extant atmosphere, supporting the prospect of fruitful future observing campaigns.

Finally, we also examined the resulting space environment around the planet candidate Proxima d, which is expected to orbit at only 0.029 au. Not surprisingly, this exoplanet would experience extreme conditions, including very large dynamic pressures (10^3–10^4 times the average value around the Earth) with sub-orbital variability reaching factors of 10, and even the possibility of sub-Alfvénic conditions for extended periods of time. A grim space weather forecast is then expected for this exoplanet candidate.

We would like to thank the referee for constructive feedback. Support for Program number HST-GO-15326 was provided by NASA through a grant from the Space Telescope Science Institute, which is operated by the Association of Universities for Research in Astronomy, Incorporated, under NASA contract NAS5-26555. J.J.D. was funded by NASA contract NAS8-03060 to the CXC and thanks the Director, Belinda Wilkes, for continuing advice and support. O.C. was supported by NASA NExSS grant NNX15AE05G. K.P. acknowledges funding from the German *Leibniz Gemeinschaft* under project number P67-2018. This work used SWMF/BATSRUS tools developed at The University of Michigan Center for Space Environment Modeling. Simulations were performed on NASA's Pleiades cluster under award SMD-17-1330, provided by the NASA High-End Computing Program through the NASA Advanced Supercomputing Division at Ames Research Center.

Facility: Pleiades.

Software: SWMF (Gombosi et al. 2018).

ORCID iDs

Julián D. Alvarado-Gómez https://orcid.org/0000-0001-5052-3473
Jeremy J. Drake https://orcid.org/0000-0002-0210-2276
Cecilia Garraffo https://orcid.org/0000-0002-8791-6286
Ofer Cohen https://orcid.org/0000-0003-3721-0215
Katja Poppenhaeger https://orcid.org/0000-0003-1231-2194
Rakesh K. Yadav https://orcid.org/0000-0002-9569-2438
Sofia P. Moschou https://orcid.org/0000-0002-2470-2109

References

Alvarado-Gómez, J. D., Drake, J. J., Fraschetti, F., et al. 2020, ApJ, 895, 47
Alvarado-Gómez, J. D., Drake, J. J., Moschou, S. P., et al. 2019a, ApJL, 884, L13
Alvarado-Gómez, J. D., Garraffo, C., Drake, J. J., et al. 2019b, ApJL, 875, L12
Alvarado-Gómez, J. D., Hussain, G. A. J., Cohen, O., et al. 2016, A&A, 594, A95
Anglada-Escudé, G., Amado, P. J., Barnes, J., et al. 2016, Natur, 536, 437
Benedict, G. F., & McArthur, B. E. 2020a, RNAAS, 4, 46
Benedict, G. F., & McArthur, B. E. 2020b, RNAAS, 4, 86
Cohen, O., Drake, J. J., Glocer, A., et al. 2014, ApJ, 790, 57
Cohen, O., Garraffo, C., Moschou, S.-P., et al. 2020, ApJ, 897, 101
Cohen, O., Glocer, A., Garraffo, C., Drake, J. J., & Bell, J. M. 2018, ApJL, 856, L11
Damasso, M., Del Sordo, F., Anglada-Escudé, G., et al. 2020, SciA, 6, eaax7467
Davenport, J. R. A., Covey, K. R., Clarke, R. W., et al. 2019, ApJ, 871, 241
Dong, C., Lingam, M., Ma, Y., & Cohen, O. 2017, ApJL, 837, L26
Finley, A. J., Matt, S. P., & See, V. 2018, ApJ, 864, 125
Fuhrmeister, B., Lalitha, S., Poppenhaeger, K., et al. 2011, A&A, 534, A133
Garcia-Sage, K., Glocer, A., Drake, J. J., Gronoff, G., & Cohen, O. 2017, ApJL, 844, L13
Garraffo, C., Drake, J. J., & Cohen, O. 2015, ApJL, 807, L6
Garraffo, C., Drake, J. J., & Cohen, O. 2016, ApJL, 833, L4
Garraffo, C., Drake, J. J., Cohen, O., Alvarado-Gómez, J. D., & Moschou, S. P. 2017, ApJL, 843, L33
Gombosi, T. I. 2004, Physics of the Space Environment (Cambridge: Cambridge Univ. Press)
Gombosi, T. I., van der Holst, B., Manchester, W. B., & Sokolov, I. V. 2018, LRSP, 15, 4
Gratton, R., Zurlo, A., Le Coroller, H., et al. 2020, A&A, 638, A120
Heller, R., Hippke, M., & Kervella, P. 2017, AJ, 154, 115
Jenkins, J. S., Harrington, J., Challener, R. C., et al. 2019, MNRAS, 487, 268
Kane, S. R., & Gelino, D. M. 2012, PASP, 124, 323
Kervella, P., Arenou, F., & Schneider, J. 2020, A&A, 635, L14
Kiraga, M., & Stepien, K. 2007, AcA, 57, 149
Kopparapu, R. K., Ramirez, R., Kasting, J. F., et al. 2013, ApJ, 770, 82
Kopparapu, R. K., Ramirez, R. M., SchottelKotte, J., et al. 2014, ApJL, 787, L29
Lugaz, N., Farrugia, C. J., Huang, C.-L., & Spence, H. E. 2015, GeoRL, 42, 4694
Moschou, S.-P., Drake, J. J., Cohen, O., et al. 2019, ApJ, 877, 105
Parkin, K. L. G. 2018, AcAau, 152, 370
Pulkkinen, T. 2007, LRSP, 4, 1
Reiners, A., & Basri, G. 2008, A&A, 489, L45
Réville, V., Brun, A. S., Matt, S. P., Strugarek, A., & Pinto, R. F. 2015, ApJ, 798, 116
Ribas, I., Bolmont, E., Selsis, F., et al. 2016, A&A, 596, A111
Ribas, I., Tuomi, M., Reiners, A., et al. 2018, Natur, 563, 365
Schield, M. A. 1969, JGR, 74, 1275
Ségransan, D., Kervella, P., Forveille, T., & Queloz, D. 2003, A&A, 397, L5
Shields, A. L., Ballard, S., & Johnson, J. A. 2016, PhR, 663, 1
Suárez Mascareño, A., Faria, J. P., Figueira, P., et al. 2020, A&A, 639, A77
Tóth, G., van der Holst, B., Sokolov, I. V., et al. 2012, JCoPh, 231, 870
Turbet, M., Leconte, J., Selsis, F., et al. 2016, A&A, 596, A112
van der Holst, B., Sokolov, I. V., Meng, X., et al. 2014, ApJ, 782, 81
Vida, K., Oláh, K., Kővári, Z., et al. 2019, ApJ, 884, 160
Vidotto, A. A., Jardine, M., Morin, J., et al. 2014, MNRAS, 438, 1162
Wargelin, B. J., & Drake, J. J. 2002, ApJ, 578, 503
Wargelin, B. J., Saar, S. H., Pojmański, G., Drake, J. J., & Kashyap, V. L. 2017, MNRAS, 464, 3281
Wood, B. E., Linsky, J. L., Müller, H.-R., & Zank, G. P. 2001, ApJL, 547, L49
Wood, B. E., Müller, H.-R., Zank, G. P., Linsky, J. L., & Redfield, S. 2005, ApJL, 628, L143
Wright, N. J., Drake, J. J., Mamajek, E. E., & Henry, G. W. 2011, ApJ, 743, 48
Yadav, R. K., Christensen, U. R., Wolk, S. J., & Poppenhaeger, K. 2016, ApJL, 833, L28